Effects of Low AIPL1 Expression on Phototransduction in Rods

Clint L. Makino,[1] Xiao-Hong Wen,[1] Norman Michaud,[1] Igor V. Peshenko,[2] Basil Pawlyk,[3] Richard S. Brush,[4,5] Maria Soloviev,[1] Xiaoqing Liu,[3] Michael L. Woodruff,[6,7] Peter D. Calvert,[1,8] Andrey B. Savchenko,[2] Robert E. Anderson,[4,5] Gordon L. Fain,[6,7] Tiansen Li,[3] Michael A. Sandberg,[3] and Alexander M. Dizhoor[2]

Purpose. To investigate the impact of aryl hydrocarbon receptor–interacting protein–like (AIPL)-1 on photoreception in rods.

Methods. Photoresponses of mouse rods expressing lowered amounts of AIPL1 were studied by single-cell and electroretinogram (ERG) recordings. Phototransduction protein levels and enzymatic activities were determined in biochemical assays. Ca^{2+} dynamics were probed with a fluorescent dye. Comparisons were made to rods expressing mutant Y99C guanylate cyclase activating protein (GCAP)-1, to understand which effects arose from elevated dark levels of cGMP and Ca^{2+}.

Results. Except for PDE, transduction protein levels were normal in low-AIPL1 retinas, as were guanylate cyclase (GC), rhodopsin kinase (RK), and normalized phosphodiesterase (PDE) activities. Y99C and low-AIPL1 rods were more sensitive to flashes than normal, but flash responses of low-AIPL1 rods showed an abnormal delay, reduced rate of increase, and longer recovery not present in Y99C rod responses. In addition, low-AIPL1 rods but not Y99C rods failed to reach the normal light-induced minimum in Ca^{2+} concentration.

Conclusions. Reduced AIPL1 delayed the photoresponse, decreased its amplification constant, slowed a rate-limiting step in its recovery, and limited the light-induced decrease in Ca^{2+}. Not all changes were attributable to decreased PDE or to elevated cGMP and Ca^{2+} in darkness. Therefore, AIPL1 directly or indirectly affects more than one component of phototransduction. (*Invest Ophthalmol Vis Sci.* 2006;47:2185–2194) DOI:10.1167/iovs.05-1341

Rod photoreceptors detect and count single photons. Their large pools of rhodopsin stand poised for photon capture. Photoexcitation of a single rhodopsin initiates a biochemical cascade by activating more than a hundred transducins.[1–3] Each transducin binds a phosphodiesterase catalytic subunit and releases it from an inhibition, allowing it to hydrolyze cGMP. As cGMP levels fall, cation channels in the plasma membrane that are gated by cGMP begin to close. The rod hyperpolarizes, and release of neurotransmitter onto second-order neurons subsides. The photocurrent response amplitude and duration are limited by the shutoff and recovery processes in the rod. Phosphorylation and arrestin binding shut off rhodopsin. PDE activity is controlled by transducin. After transducin hydrolyzes its bound GTP, transducin and the PDE bound to it become inactive. cGMP levels are restored by GC. The rate of synthesis is subject to negative feedback control, triggered by the decline in intracellular Ca^{2+} that occurs after closure of the cGMP-gated channels. In low Ca^{2+}, guanylate cyclase activating proteins (GCAPs) quicken the recovery by stimulating GC to produce cGMP at a faster rate.

Disturbances in cGMP metabolism have been linked to several degenerative retinal diseases[4,5] (http://www.sph.uth.tmc.edu/RetNet/disease.htm/ provided in the public domain by the University of Texas Houston Health Science Center, Houston, TX). Mutations in AIPL1, the putative specialized chaperone required for proper expression of PDE in rods,[6,7] give rise to Leber congenital amaurosis.[8,9] In one form of cone–rod dystrophy a Y99C mutation in GCAP1[10] shifts its inhibitory effect on cGMP synthesis to very high Ca^{2+} levels that normally lie outside the physiological range.[11–13] As a result, the light-induced increase in guanylate cyclase activity persists for a longer period after photon absorption. In transgenic mice expressing Y99C GCAP1 or that have reduced expression of AIPL1, rods appear to equilibrate at elevated levels of free cGMP and Ca^{2+} in darkness. In this report, we compared the properties of low-AIPL1 rods to those of Y99C GCAP1 rods. The latter rods provided an important positive control for heightened levels of cGMP and Ca^{2+} in darkness, which affect phototransduction directly and possibly also indirectly (e.g., by changing the expression levels of certain proteins). Our results indicated that low AIPL1 does more than simply affect levels of PDE expression.

Methods

Mice with reduced expression of AIPL1 and mice expressing Y99C GCAP1 on a wild-type (WT) background were generated.[6,14] The experiments on Y99C mice were performed on the L52H and L53

From the [1]Howe Laboratory and [3]Berman-Gund Laboratory for the Study of Retinal Degenerations, Department of Ophthalmology, Massachusetts Eye and Ear Infirmary and Harvard Medical School, Boston, Massachusetts; [2]Hafter Research Laboratories, Pennsylvania College of Optometry, Elkins Park, Pennsylvania; the Departments of [4]Cell Biology and [5]Ophthalmology, University of Oklahoma College of Medicine, Oklahoma City, Oklahoma; and the [6]Department of Physiological Science and [7]Jules Stein Institute, University of California at Los Angeles, Los Angeles, California.

[8]Present address: Department of Ophthalmology, University of Pennsylvania, Philadelphia, Pennsylvania.

Supported by National Eye Institute Grants EY11358 and EY12944 (CLM); EY11522 (AMD); EY00871, EY04149, and EY12190 (REA); EY10309 (TL); EY01844 (GLF); and EY014104 (core grant to Massachusetts Eye and Ear Infirmary). AMD is the Martin and Florence Hafter Professor of Pharmacology.

Submitted for publication October 12, 2005; revised December 7, 2005; accepted February 27, 2006.

Disclosure: **C.L. Makino**, None; **X.-H. Wen**, None; **N. Michaud**, None; **I.V. Peshenko**, None; **B. Pawlyk**, None; **R.S. Brush**, None; **M. Soloviev**, None; **X. Liu**, None; **M.L. Woodruff**, None; **P.D. Calvert**, None; **A.B. Savchenko**, None; **R.E. Anderson**, None; **G.L. Fain**, None; **T. Li**, None; **M.A. Sandberg**, None; **A.M. Dizhoor**, None

The publication costs of this article were defrayed in part by page charge payment. This article must therefore be marked "*advertisement*" in accordance with 18 U.S.C. §1734 solely to indicate this fact.

Corresponding author: Clint L. Makino, Department of Ophthalmology, Harvard Medical School and the Massachusetts Eye and Ear Infirmary, 243 Charles Street, Boston, MA 02114; cmakino@meei.harvard.edu.

lines, in which expression of the mutant GCAP1 relative to endogenous was 1:1 to 2:1 and 3:1 to 4:1, respectively.[14] All experiments conformed to the ARVO Statement for the Use of Animals in Ophthalmic and Vision Research.

Physiological Methods

Methods for recording responses from single cells, the ERG and the intracellular concentration of free Ca^{2+} have been described previously.[6,14] Some of the experiments were performed on the mice in those studies.[6,14] Statistics were analyzed by computer (Stata, ver. 6; Stata Corp., College Station, TX; and JMP, ver. 3.2, or PROC MIXED of SAS, ver. 6.12; SAS Institute, Cary, NC).

Electron Microscopy

Enucleated eyes from 4- to 6-week-old low-AIPL1 mice and sibling controls were fixed with 2.5% glutaraldehyde and 2% formaldehyde in 0.1 M cacodylate buffer with 0.08 M $CaCl_2$ at 4°C. The tissue was postfixed in 2% aqueous OsO_4 and then with 2% aqueous uranyl acetate. Tissue was dehydrated in graded ethanols, transitioned in propylene oxide, and embedded in Epon. One-micrometer-thick sections were stained with toluidine blue in borate buffer. Sections, 70 to 90 nm in thickness, were stained with uranyl acetate and Sato's lead stain and examined on an electron microscope (CM-10; Philips, Eindhoven, The Netherlands).

Biochemical Analyses

Retinas were harvested from mice under infrared illumination after at least 18 hours of dark adaptation. A sample was removed for the spectrophotometric quantification of rhodopsin content. Other samples were subjected to polyacrylamide gel electrophoresis and transferred to membranes (Immobilon-FL; Millipore, Billerica, MA). The membranes were incubated with anti-PDE (1:1000; CytoSignal, Irvine, CA), anti-recoverin (1:50,000, P26),[15] or anti-RGS9 (1:1,000, a gift from Theodore G. Wensel, Baylor College of Medicine, Houston, TX) antibodies followed by fluorochrome-conjugated goat anti-rabbit IgG (1:5000, IRDye800; Rockland Immunochemicals, Gilbertsville, PA) and analyzed with an infrared imaging system (Odyssey; LI-COR Biotechnology, Lincoln, NE).

For measurements of light-activated PDE activity, rod outer segment (ROS) membranes were prepared with proteinase inhibitors (Complete Mini, EDTA-free Proteinase Inhibitor Cocktail; Roche Applied Science, Indianapolis, IN). Membranes containing ~40 picomoles rhodopsin were incubated with 50 units of streptolysin O (Sigma-Aldrich, St. Louis, MO) for 5 minutes at 30°C. In some samples, >99% of the rhodopsin was bleached with ~4000 lux from an incandescent source for 30 seconds on ice. Otherwise, all procedures through PDE quenching were observed under infrared illumination. Cyclic GMP hydrolysis was performed in (mM): KCl, 48; NaCl, 6.4; $MgCl_2$, 5; dithiothreitol, 0.8; EGTA, 0.008; Tris, 40 (pH 7.5), with initial concentrations of (mM): 5′GMP, 2; GTP, 1; cGMP, 4, and including ~0.5 μCi ^{3}[H]cGMP (PerkinElmer Life Sciences, Emeryville, CA). The reaction was quenched after 5 minutes by heating at 95°C for 2 minutes. The mixture was chilled on ice for 5 minutes and centrifuged at 12,000*g*. Cyclic GMP and the reaction product, 5′GMP were separated by thin-layer chromatography and quantified on a liquid scintillation counter.[16,17] To determine the maximum PDE activities, low-AIPL1 and WT ROS membranes were first subjected to trypsinization and diluted 8.9-fold. In baseline studies of 2.5-, 5-, 10-, and 15-minute exposures to trypsin, 10-minute digests yielded the highest PDE activities in both low-AIPL1 and WT samples. Trypsin was inactivated with 50 mM phenylmethylsulfonyl fluoride (PMSF). Levels of transducin (n = 2 determinations) and PDE (n = 3 determinations) in the low-AIPL1 ROS membrane samples relative to those in WT were measured as described earlier.

Light-induced translocation of transducin was detected by immunofluorescence in two pairs of low-AIPL1 and WT mice.[6]

Rhodopsin phosphorylation was evaluated with an assay[18] on ROS using anti-phospho-Ser334 and -Ser338 rhodopsin antibodies.[19] Fluorochrome-conjugated goat anti-rabbit secondary antibody was applied and the membranes scanned (Odyssey; LI-COR Biotechnology).

Retinal GC activity was determined for low-AIPL1 and WT ROS according to Olshevskaya et al.[14]

Lipid Analysis of Disc Membranes

Disc membranes were prepared from retinas of dark-adapted mice.[20] Rhodopsin concentration was quantified spectrophotometrically. Lipids were extracted twice from disc membranes in a 1:1:1 mixture of chloroform-methanol-water and once more from a 3:48:47 mixture. The purified lipid extract was stored under N_2 in a known volume of chloroform-methanol (1:1).

Fatty acids were esterified and subjected to gas chromatographic analysis.[21–24] A mixture of pentadecanoic acid (15:0), heptadecanoic acid (17:0), and heneicosanoic acid (21:0) was added as an internal standard. The mixture was dried under N_2 then solubilized in toluene and 2% H_2SO_4 in methanol. The mixture was sealed under N_2, vortexed, and heated at 100°C for 60 minutes. Tubes were cooled on ice and 1.2 mL H_2O was added. The fatty acid methyl esters were extracted three times with 2.4 mL hexane, dried under N_2, and dissolved in 20 μL nonane. The fatty acid compositions were determined by injecting 3 μL at 250°C with the split ratio set to 5:1 using a DB-225 capillary column (30 m × 0.53 mm inner diameter; J&W Scientific, Folsom, CA) in a gas chromatograph (6890N; Agilent, Wilmington, DE). The column temperature began at 160°C and ramped 1.33°C min^{-1} to 220°C, where it was held for 18 minutes. Hydrogen carrier gas flowed at 5.3 mL min^{-1} and the flame ionization detector temperature was set to 270°C. The chromatographic peaks were integrated and processed (ChemStation software; Agilent Technologies, Palo Alto, CA). Fatty acid methyl esters were identified by comparison of their relative retention times with authentic standards.

Results

Enhanced Photoresponses in Low-AIPL1 Mice

Overall, flash responses from low-AIPL1 and Y99C L52H rods did not differ greatly from those of WT (Fig. 1). Both types of mutant rods tended to be more sensitive, requiring fewer photons to elicit a half-maximum response. As in Y99C rods, the single-photon response in low-AIPL1 rods was probably also larger than normal (Fig. 2), to account for the higher sensitivity in the face of reduced outer segment diameter (described later), which would have decreased quantal catch. That difference was not resolved in the small number of cells sampled. An overshoot was observed in each of 12 Y99C L52H rods (e.g., Fig. 1A) and in half of the L53 rods recorded. Overshoots were smaller and occurred less frequently in low AIPL1 and WT rods.

The rising phase of the single-photon response in Y99C L52H rods was normal except that it continued for an extra 30 ms (Fig. 2). The single-photon response in low-AIPL1 rods also had a longer time to peak, but it rose ~50% more gradually. The final segment of the dim flash response recovered exponentially with a similar time constant (τ_r) for L52H and WT rods. The time constant for low-AIPL1 rods was approximately two times slower. Integration time was unaffected for Y99C rods but was greater in low-AIPL1 rods, reflecting their slower response recovery.

For bright flashes, response saturation time increased linearly with the logarithm of the flash strength.[25,26] The slope of the saturation function (τ_c) was greater for low-AIPL1 rods. The increases in τ_c obtained from bright flashes and in τ_r determined from dim flashes signify a slower rate-limiting step in the recovery of the photoresponse[25,26] for low-AIPL1 rods. Slowed recovery in low-AIPL1 rods appeared to be unrelated to ele-

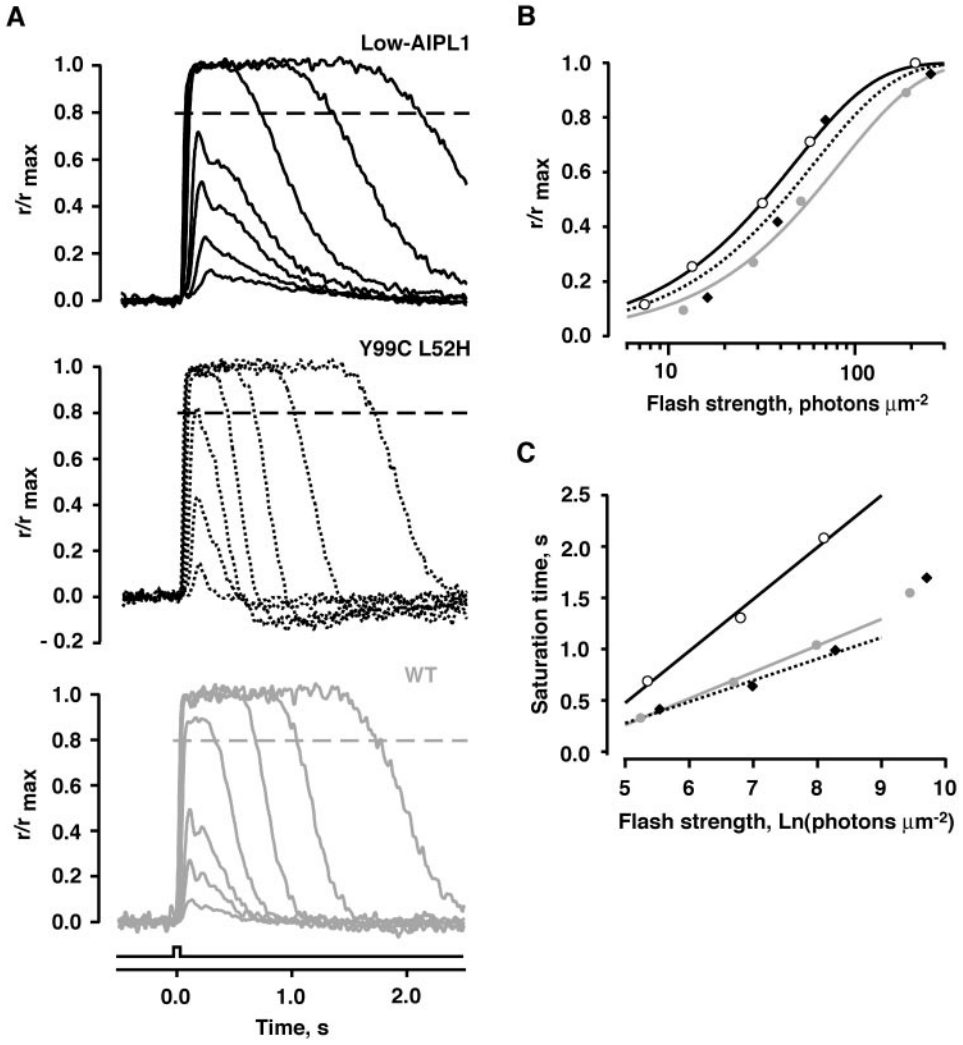

FIGURE 1. Comparison of flash responses. (**A**) Averaged responses to flashes of increasing strength. *Bottom trace*: the flash monitor. r_{max} was 9.1, 9.6, and 10.7 pA for low-AIPL1, L52H, and WT, respectively. The flash strengths at 500 nm were (photons μm^{-2}): 7, 13, 32, 57, 210, 897, and 3,290 for low-AIPL1; 16, 39, 70, 254, 1,080, 3,940, and 16,400 for L52H; and 12, 28, 51, 188, 803, 2,940, and 12,600 for WT. (**B**) Relation between response and flash strength: low-AIPL1 (*open circles*), Y99C L52H (*filled diamonds*), and WT (*shaded circles*). Results were fitted with: $r/r_{max} = 1 - \exp(-ki)$, where r is response amplitude, i is flash strength, and k is a constant, for the cells in (**A**). Points corresponding to the strongest flashes are not shown. (**C**) Pepperberg plots for the rods in (**A**). Symbols for rod type are the same as in (**B**). Saturation time was measured from midflash to 20% recovery, as shown by the *dashed lines* in (**A**). Linear regression of the initial segments yielded slopes of: 505 ms for low-AIPL1, 209 ms for L52H, and 277 ms for WT rods.

vated cGMP or Ca^{2+} in darkness because τ_c and τ_r were normal in Y99C rods. Averaged results are summarized in Table 1.

Better resolution of the rising phase of the low-AIPL1 photoresponse was obtained in electroretinographic recordings of the initial, corneal negative a-wave, which summates the photocurrent responses of many rods (Fig. 3). The response to a saturating flash was fit with[27]

$$R = R_{max}\{1 - \exp[-0.5\Phi A(t - t_{eff})^2]\}, \quad (1)$$

where R is a-wave amplitude, Φ is the number of photoisomerizations, A is the amplification constant of phototransduction, and t_{eff} is the latency from flash to the onset of the a-wave. On average, t_{eff} was 0.44 ms longer in low-AIPL1 mice.[6] In addition, the trajectory of the a-wave in low-AIPL1 mice was more gradual due to a ~30% decrement in the amplification constant (Fig. 3B). That the changes in latency and amplification constant of the flash response were caused by the decrease in low-AIPL1 and not by elevations in cGMP, and Ca^{2+} was

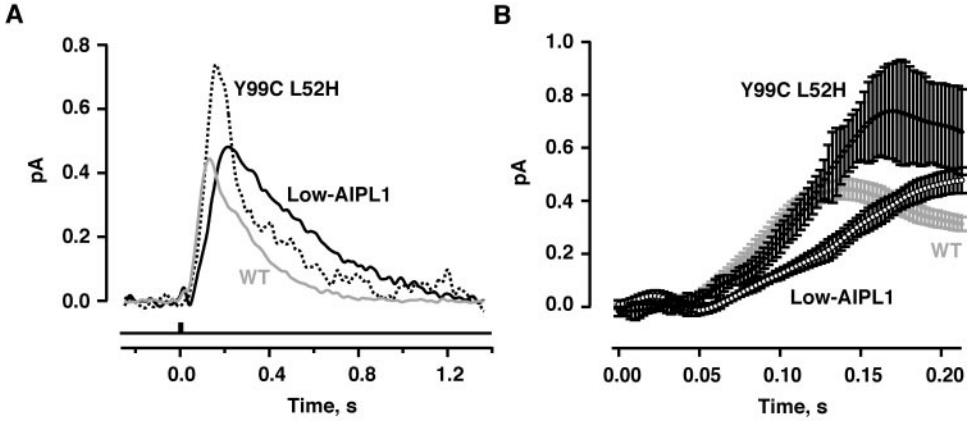

FIGURE 2. Single-photon responses of low-AIPL1, Y99C L52H and WT rods. (**A**) For each rod, the dim flash response was scaled to the ratio of the ensemble variance to the mean amplitude. Traces show averages from 15 low-AIPL1, 8 Y99C L52H, and 27 WT rods. Results from Liu et al.[6] and Olshevskaya et al.[14] have been included in the WT and low-AIPL1 averages. (**B**) Expanded view of the rising phases of the responses from (**A**). No corrections were made for the delay in the response imposed by low-pass filtering during data acquisition. Error bars, SEM.

TABLE 1. Flash Response Properties from Single-Cell Recordings

	Low-AIPL1	Y99C L52H	Y99C L53	WT
$i_{0.5}$ (photons μm^{-2})	30 ± 1 (54)* <0.001	45 ± 3 (12) NS	39 ± 6 (11)† NS	51 ± 2 (43)*†
Single-photon response				
Amplitude (pA)	0.56 ± 0.05 (5) NS	0.81 ± 0.18 (8) 0.026	0.85 ± 0.13 (9) 0.008	0.45 ± 0.04 (27)
Time to peak (ms)	232 ± 8 (43)* <0.001	170 ± 6 (12) NS	206 ± 14 (11) 0.001	138 ± 7 (40)
Integration time (ms)	467 ± 25 (40)* <0.001	367 ± 67 (12) NS	282 ± 18 (11) NS	303 ± 26 (40)
Recovery time constant, τ_r (ms)	495 ± 62 (33) 0.006	395 ± 108 (12) NS	165 ± 47 (5) NS	230 ± 34 (33)
Saturation time constant, τ_c (ms)	428 ± 25 (36) <0.001	255 ± 28 (12) NS	276 ± 56 (5) NS	270 ± 14 (33)

Data are given as the mean ± SEM, (*n*) *P* where the probability was obtained from an ANOVA followed by a Scheffé test to compare mutant against control parameters. NS, not significant. $i_{0.5}$, the flash strength eliciting a half-maximum response, varies inversely with sensitivity. Single-photon response amplitude was estimated by dividing the ensemble variance by the mean dim flash response amplitude. Kinetics of the single photon response were determined from dim flash responses with amplitudes less than one fifth of the maximum. Time to peak was measured from midflash to the response peak. Integration time was calculated as the integral of the response divided by response amplitude. Recovery time constant refers to a fit of the final declining phase of the dim flash response with a single exponential. Saturation time constant is the slope of the relation between saturation time and the natural logarithm of the flash strength, by linear regression (cf. Fig. 2).

* Includes results reported in Liu et al.[6]

† Includes results from Olshevskaya et al.[14]

suggested by their absence in a limited number of Y99C L52H single cell (Fig. 2B) and ERG recordings (not shown).

By 8 to 20 weeks, the maximum amplitude of the a-wave was reduced in low-AIPL1 mice by approximately 25%, reflecting a loss of rods. Relative sensitivity was somewhat higher than normal, based on the fractional response to a bright flash. The time to peak or implicit time of the a-wave was longer than that of WT. Age had no interactive effect with mouse type on the latency or the amplification constant of the a-wave. Averaged results are listed in Table 2. With pairs of very bright flashes, low-AIPL1 mice required longer interstimulus intervals for recovery (Fig. 3C), consistent with the increased saturation time observed in single-cell recordings of low-AIPL1 rods (Fig. 1).

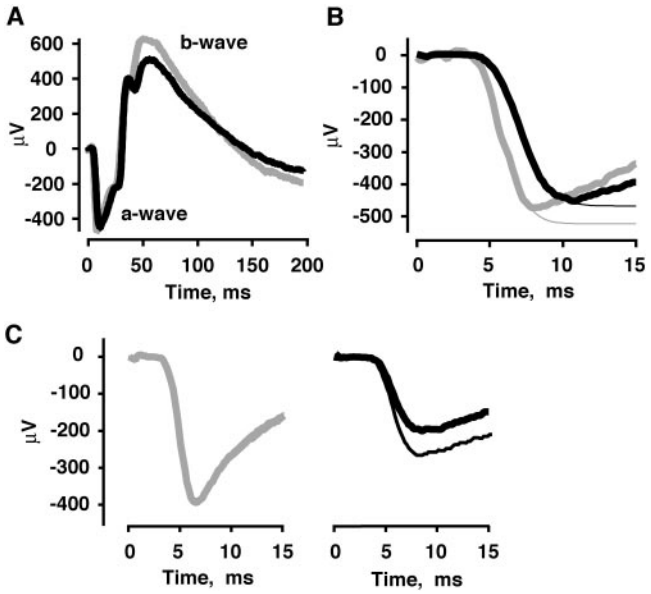

FIGURE 3. ERG responses from low-AIPL1 (*black traces*) and WT (*gray traces*) mice. (**A**) A saturating, 28-fL/s flash of white light, producing an estimated 11,700 photoisomerizations per rod, was given at time 0. Each trace represents a single trial in mice at 5 to 6 weeks of age. (**B**) Expanded view of the a-waves (*thick lines*). The time to the peak of the a-wave was greater for the low-AIPL1 mice. Fittings with equation 1 (*thin lines*) yielded $A = 24$ seconds^{-2} and $t_{eff} = 3.68$ ms for the WT mouse, whereas for the low-AIPL1, $A = 16$ seconds^{-2} and $t_{eff} = 4.38$ ms, respectively. (**C**) Responses to paired saturating flashes of 90 fL/s delivered 4 minutes apart in 12- to 20-week-old mice. The maximum a-wave amplitude was reduced in low-AIPL1 mice at this age. In WT, the response to each of the flashes had the same amplitude (*left*), but in low-AIPL1, the response to the second flash (*right*, *thick trace*) was less than the response to the first (*right*, *thin trace*).

Morphology

Because response kinetics are affected by cytoplasmic volume,[27,28] we inspected the ultrastructure of low-AIPL1 rods (Fig. 4B). The disc-to-disc repeat distance of 310 ± 5 Å in WT increased to 331 ± 4 Å in low-AIPL1 (mean ± SEM, $n = 50$ rods each). The difference in low-AIPL1 rods appeared to arise mainly from swelling of some of the disks rather than from an increase in their separation. In sections taken tangential to the retina, there was a slight reduction in rod outer segment diameter from 1.44 ± 0.02 μm ($n = 59$) in WT to 1.32 ± 0.02 μm ($n = 59$) in low-AIPL1 that would decrease cytoplasmic volume in the latter by 16%.

Analyses of Protein Expression and Activity and Disc Membrane Composition

In 12 assays of samples from six pairs of low-AIPL1 and WT mice at 4 to 10 weeks, the amount of PDE in low-AIPL1 retinas was 29% ± 2% of that in WT retinas (Fig. 5A). The result is similar to the 20% ± 1% ($n = 6$ pairs of mice) obtained by a different method.[6] In assays of cGMP hydrolysis by PDE, light-induced, as well as maximum trypsin-induced activity in low-AIPL1 ROS were lowered in proportion to the amount of PDE present (Fig. 5D). Thus, although low-AIPL1 rods expressed less PDE, all PDE molecules were fully functional.

The amount of transducin,[6] as well as its light-dependent movement, were normal in low-AIPL1 mice. Nearly all the transducin was localized in the outer segments of dark-adapted rods, and it redistributed to the rod inner segments and synaptic terminals after exposure to bright light in both types of mice (Fig. 6).

TABLE 2. Characterization of the ERG

	Low-AIPL1	WT
a-Wave latency, t_{eff} (ms)	4.49 ± 0.10 (8)	4.05 ± 0.09 (9)
	0.007	
Log A (s^{-2})	1.16 ± 0.03 (8)	1.33 ± 0.04 (9)
	0.007	
a-Wave implicit time (μs)	22.4 ± 0.4 (10)	17.8 ± 0.3 (10)
	<0.0001	
Maximum a-wave amplitude (μV)		
5 to 6 weeks of age	−406 ± 14 (8)	−445 ± 22 (9)
	NS	
8 to 20 weeks of age	−311 ± 26 (9)	−429 ± 29 (10)
	0.008	

Data are given as the mean ± SEM, (*n*) *P* where the probability was obtained from a *t*-test. NS, not significant. The a-wave latency and *A*, the amplification constant, were determined in the mice from Liu et al.[6] at 5 to 6 weeks of age by a fitting of saturating flash responses with equation 1 as shown in Figure 3. Geometric means were computed for the amplification constant because of the skewness. Implicit times were measured in different mice at 8 to 20 weeks with a subsaturating flash of 0.2 fL/s that produced an estimated 80 photoisomerizations per rod.

Although low-AIPL1 mice express the normal amounts of rhodopsin kinase[6] and recoverin (104% ± 9%, six determinations in four pairs of mice, Fig. 5B), improper processing of the proteins could slow the response recovery. However, in ROS exposed to steady light for various periods, there was no indication of a defect in rhodopsin shutoff (Fig. 5E). The rate of rhodopsin phosphorylation at ser334 in low-AIPL1 relative to that in WT was 120% ± 0.05% and that at ser338 was 109% ± 0.02% (four determinations at each site). Knockout of the regulator of G-protein signaling-9 (RGS9) slows the flash response recovery,[29] but in low-AIPL1 rods, the relative RGS9 expression was 109% ± 4% (five determinations in three pairs of mice; Fig. 5C).

Rhodopsin concentration can affect photoresponse kinetics[20] (although, cf. Liang et al.[30]). However, there were 74 ± 3 phospholipids per rhodopsin in low-AIPL1 preparations (n = 3), compared with 75 ± 9 in WT (n = 4), indicating that the rhodopsin concentration was normal. Early changes in fatty acid composition of retinas from *rd1* mice have been reported.[31] Fatty acid content could slow activation and shutoff rates of phototransduction by diminishing membrane fluidity. No changes that would affect membrane fluidity were observed in low-AIPL1 rod disc membranes: the average fatty acyl chain length was 19.7 ± 0.2 carbon atoms (19.3 ± 0.3 for WT), the average number of double bonds per fatty acid was 2.9 ± 0.2 (2.5 ± 0.5 for WT), and the ratio of saturated to unsaturated fatty acids was 0.7 ± 0.1 mol mol^{-1} (1.2 ± 0.5 for WT). Analysis of the disc membranes from a single sample of L52H mice gave no indication of a change in fatty acid composition.

Expression levels of GCAPs affect the Ca^{2+} dependence of cGMP production and photoresponse kinetics[14,32,33] and a decrease in Ca^{2+}-sensitive GC activity accompanies downregulation of PDE in other transgenic mice.[34] But in low-AIPL1 rods, maximum GC activity and the dependence of activity on Ca^{2+} were unchanged (Fig. 7). The shifts in GC activities of Y99C retinas to higher Ca^{2+} concentrations[14] are shown for comparison.

Alterations in Intracellular Ca^{2+}

The accumulation of cGMP in low-AIPL1 and in Y99C rods opens a greater fraction of cGMP-gated channels and supports a higher influx of Ca^{2+}. The geometric mean Ca^{2+} concentrations from the results of Liu et al.[6] and Olshevskaya et al.[14] were 210 nM in WT rods and 360 nM in Y99C L53 rods. The Ca^{2+} concentrations in low-AIPL1 and in L52H rods rested at intermediate levels, but statistical significance was not observed, because the magnitude of the differences from WT were relatively small (Table 3).

After a delay, the initial rate of light-induced Ca^{2+} decline was similar for low-AIPL1, L52H, and WT rods (Fig. 8). There was a longer delay and slower Ca^{2+} decline in L53 rods, possibly due to severe disruptions in their outer segment ultrastructure (Fig. 4), or because the large excess of GCAP1 served as a rapidly exchanging Ca^{2+} buffer.

In contrast to WT rods, Ca^{2+} in low-AIPL1 rods only dropped to ~80 nM, with no sign of any small, protracted decline over an ensuing 100-second period. The restricted

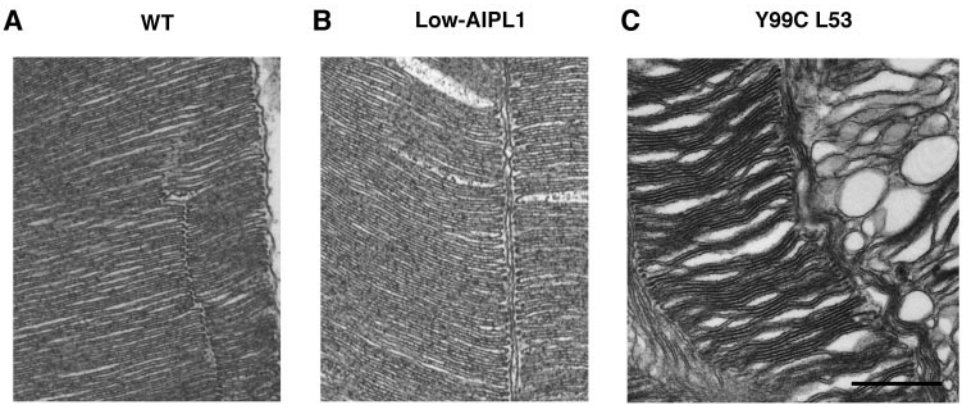

FIGURE 4. Outer segments of WT, low-AIPL1 and Y99C L53 photoreceptors. (**A**) A WT rod outer segment with disks stacked neatly. (**B**) Two low-AIPL1 rods with nearly normal morphology. There were occasional swollen disks. (**C**) Two L53 outer segments with abnormal disc structure. Some disks in the rod on the *left* were collapsed, whereas others were swollen. Disc bloating was most drastic for the cell on the *right*. Scale bar, 0.5 μm.

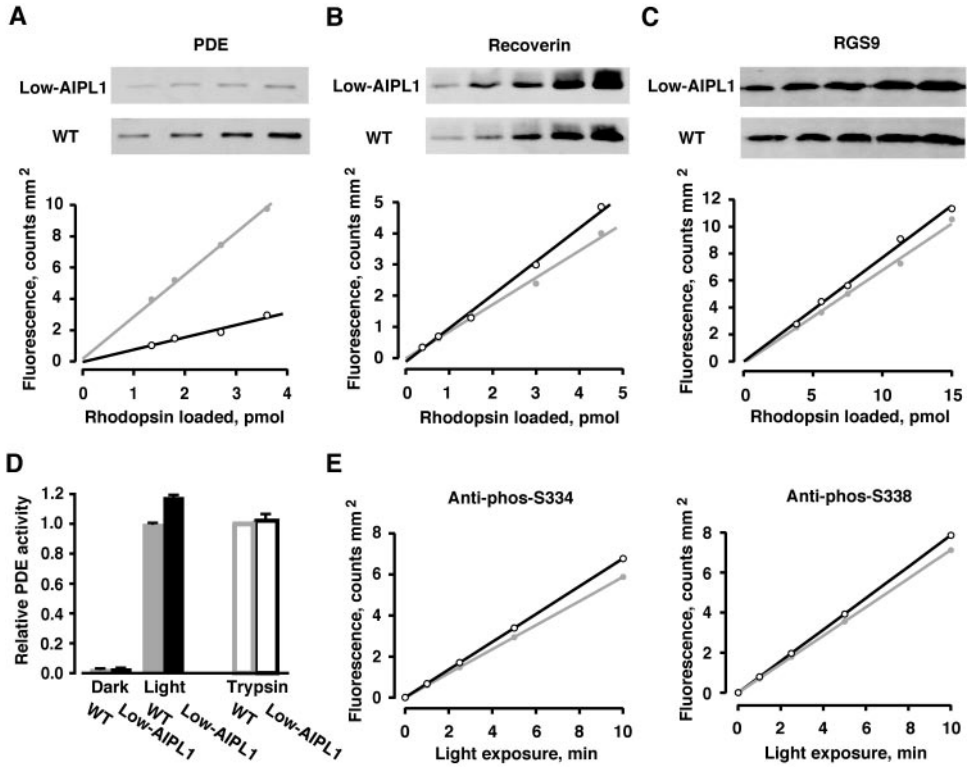

FIGURE 5. Assessment of the levels of (**A**) PDE, (**B**) recoverin, and (**C**) RGS9 in low-AIPL1 rods (*black*) relative to WT (*gray*). The relation between fluorescence and protein level (picomoles of rhodopsin loaded) was found by linear regression. The ratio of the slopes yielded the amount of protein in the low-AIPL1 sample relative to that in WT: 0.3, 1.2, and 1.1 for PDE, recoverin and RGS9, respectively. (**D**) Normal specific activity of PDE in outer segment membranes of low-AIPL1 rods. Basal and light-activated PDE activities were determined in parallel, so mean values were normalized for PDE content and then compared to that of light-activated WT samples (*open gray bar*). For maximum activity, there were several separate determinations of paired WT and low-AIPL1 samples after trypsin activation, so the mean ratio is plotted (*open black bar*). Error bars, SEM; two determinations for each sample in darkness, three determinations each for samples activated by light and by trypsin. (**E**) Similar rates of rhodopsin phosphorylation in low-AIPL1 (*black*) and WT (*gray*) rod outer segments. The ratios of the slopes were 1.15 and 1.08 for phosphorylation at ser334 and ser338, respectively.

Ca^{2+} fall in low-AIPL1 rods was not simply due to a higher resting level in darkness, because Ca^{2+} fell to the normal level in L52H and L53 Y99C rods. For an unknown reason, in low-AIPL1 rods, the $Na^+/K^+,Ca^{2+}$ exchanger operated poorly at low Ca^{2+} or Ca^{2+} continued to enter the outer segment, even after cGMP declined to low levels. Averaged results are summarized in Table 3.

Discussion

On complete AIPL1 ablation, PDE decreases to 10% of WT level.[7] The residual PDE shows no light-activated activity in biochemical assays or by ERG, and cGMP increases to higher than normal concentrations that can trigger the onset of degenerative events. The proportionate declines in rod PDE and AIPL1 proteins without a reduction in mRNA level for any of the PDE subunits suggests that AIPL1 serves as a special chaperone for rod PDE.[6] Abnormalities in the photocurrent responses reveal several mechanistic features of phototransduction, although some seem unrelated to the shortage of PDE.

The Collision Time for Transducin-PDE

In normal rods, a latency (t_{eff}) separates photon absorption from the onset of the photoresponse. The latency includes the times required for rhodopsin to transform into the catalytically active state (t_R), rhodopsin to bind and activate transducin (t_G), transducin to bind and activate PDE (t_{PDE}), cGMP to decline (t_{cGMP}), and channels to close (t_{chan})[27]

$$t_{eff} = t_R + t_G + t_{PDE} + t_{cGMP} + t_{chan} \quad (2)$$

With 3.4- to 5-fold lower PDE, the separation of transducin on the disc membrane surface from the nearest PDE lengthens by the square root of the change in PDE concentration, approximately twofold. If collision time dominates t_{PDE}, then it will also increase by twofold. Subtracting the latency of WT rods from that of low-AIPL1 rods,

$$0.44 \text{ ms} = 2\, t_{PDE} - t_{PDE} \quad (3)$$

yields t_{PDE} = 0.44 ms. In ERG recordings of WT mice, we observed a t_{eff} of 4.0 ms, similar to the values of 3.1 to 3.4 ms determined by others.[35,36] Accordingly, ~10% of the delay in phototransduction arises from the collision time between transducin and PDE in normal mouse rods.

Inefficient Transducins?

After emerging from the baseline, the photon response may be characterized by an amplification constant, A[27]:

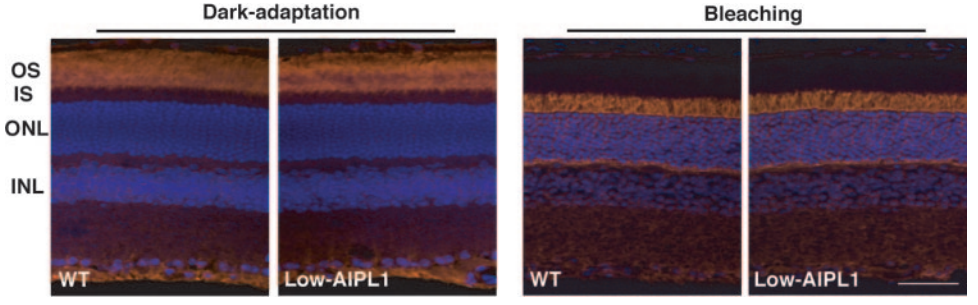

FIGURE 6. Translocation of transducin in retinas of low-AIPL1 mice after exposure to intense light for 15 minutes. Labeling of the rod transducin α-subunit is shown in *orange*. Cell nuclei were stained *blue* with Hoechst dye 33342. Scale bar, 30 μm.

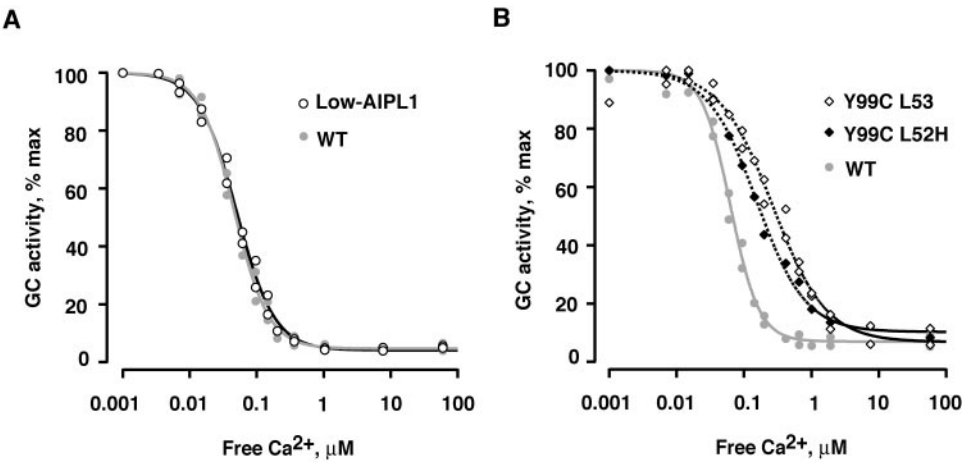

FIGURE 7. Ca^{2+}-dependence of guanylate cyclase activity. (**A**) Normal relation for low-AIPL1 retinas. $K_{m,Ca}$ and Hill coefficients were: 46 ± 5 nM and 1.69 ± 0.01 (two determinations) for WT and 50 ± 5 nM and 1.54 ± 0.01 (n = 2) for low-AIPL1. The maximum activity at low Ca^{2+}(≪5 nM) for low-AIPL1 was 0.276 ± 0.006 nanomoles cGMP min^{-1} $retina^{-1}$ (five determinations) and the minimum activity at high Ca^{2+} (50 mM) was 0.0144 ± 0.0000 (n = 2), values similar to those for WT: 0.295 ± 0.002 (n = 5) and 0.0155 ± 0.005 nanomoles cGMP min^{-1} $retina^{-1}$ (n = 2). (**B**) Shift in activity to higher Ca^{2+} with Y99C expression. $K_{m,Ca}$ were: 63 ± 5 nM (n = 2), 154 (n = 1), and 268 ± 59 (n = 2) nM, and Hill coefficients were: 2.0 ± 0.1, 1.2, and 1.10 ± 0.01 for WT, Y99C L52H, and Y99C L53, respectively. Modified with a minor correction of one Ca^{2+} concentration from Olshevskaya EV, Calvert PD, Woodruff ML, et al. The Y99C mutation in guanylyl cyclase-activating protein 1 increases intracellular Ca^{2+} and causes photoreceptor degeneration in transgenic mice. *J Neurosci.* 2004;24:6078–6085. © 2004, Society for Neuroscience.

$$A = \nu_{RG} c_{GP} \beta n, \quad (4)$$

where ν_{RG} is the rate with which a photoexcited rhodopsin activates transducins, c_{GP} is the probability that an activated transducin will couple with PDE, β is the rate constant for cGMP hydrolysis by a PDE catalytic subunit, and n is the Hill coefficient for the cGMP-gated channel. The 32% reduction in the low-AIPL1 amplification constant, determined from the a-wave, indicates that one or more factors in equation 4 decreased. The true magnitude of decrease was 1.19 (32%), or ~40%, because β is inversely proportional to cytoplasmic volume,[27,28] which was reduced in low-AIPL1 rods by the factor (1.44 μm/1.32 μm)^2, based on measurements of ROS diameters. Modeling of the photon response provided additional support for a reduction in the amplification constant in low-AIPL1 rods (Fig. 9 and Appendix).

Neither AIPL1 nor PDE is known to interact with the cGMP-gated channel. Because the leading edge of the a-wave and the photoresponse are attenuated by isobutylmethylxanthine, a PDE inhibitor,[40,41] imperfect folding of PDE in low-AIPL1 rods could have decreased β. However, the cGMP hydrolytic activity in low-AIPL1 rods fell in proportion to the reduction in PDE content. Apparently, low levels of AIPL1 were adequate for the proper folding of the entire complement of PDE expressed.

ν_{RG} depends on the collision time between rhodopsin and transducin, which is affected by their concentrations.[20] The normal phospholipid-to-rhodopsin ratio in low-AIPL1 disc membranes ruled out a difference in the packing density of rhodopsin. Nor was there a shift in membrane composition that could alter membrane fluidity. Expression level and localization were unchanged for transducin and the light-dependent movement of transducin between inner and outer segments appeared to be intact (Fig. 6). Nevertheless, preservation of transducin's high affinity for photoexcited rhodopsin and rapid nucleotide exchange should be confirmed before a decrease in ν_{RG} is ruled out, particularly after the demonstration that AIPL1 can interact with the γ-subunit of transducin.[42]

Another consideration is that the 6- to 13-fold excess of PDE over the RGS9 complex in normal rods ensures a high success rate for the collision of activated transducins with PDE.[43–45] In low-AIPL1 rods, the ratio reduced to 1- to 4-fold, increasing the probability that transducin would collide with an RGS9 instead of a PDE. It has been argued that the low affinity of transducin for the RGS9 complex in the absence of PDEγ prevents premature shutoff of transducin.[46] In the intact rod, random diffusional motion of RGS9 and transducin on the membrane surface may keep the interacting entities in proximity long enough to overcome the low affinity. If transducin must dissociate from RGS9 before binding PDE, then RGS9 will effectively delay the availability of active transducins as if there were a decline in ν_{RG}. Some transducins will shut off without ever activating PDE, thus lowering c_{GP}. The 40% decrease in pho-

TABLE 3. Dynamics of Intracellular Free Ca^{2+}

	Low-AIPL1	Y99C L52H	Y99C L53	WT
Log[Ca^{2+}] in darkness (nM)	2.41 ± 0.09 (12)	2.44 ± 0.05 (10)	2.56 ± 0.06 (10)	2.32 ± 0.03 (56)
	NS	NS	0.01	
Delay in the fall in Ca^{2+} (ms)	33 ± 11 (12)	44 ± 14 (14)	97 ± 63 (10)	34 ± 13 (21)
	NS	NS	<0.001	
Exponential decline in Ca^{2+}				
τ_1 (ms)	106	94	185	67
τ_2 (ms)	432	340	513	318
Log[Ca^{2+}] in the light (nM)	1.89 ± 0.09 (12)	1.59 ± 0.05 (10)	1.64 ± 0.09 (10)	1.56 ± 0.03 (55)
	<0.0002	NS	NS	

Data are given as the mean ± SEM, (n) P where the probability was obtained from an analysis of variance followed by the Dunnett test for the Log[Ca^{2+}] and by the Scheffé test for the delay in the decline in Ca^{2+}. NS, not significant. Log[Ca^{2+}] in darkness and in the light were compared because the populations were skewed. Log[Ca^{2+}] was calculated from results published before.[6,14] The delay was measured from the beginning of laser exposure until a 10% decline. For many rods, fitting of the decline in Ca^{2+} with a double-exponential function was very sensitive to the number of points included in the fit. Therefore, the normalized Ca^{2+} declines for rods of a given type from the delay to 1 s after laser exposure were averaged (Fig. 8) before determining the time constants.

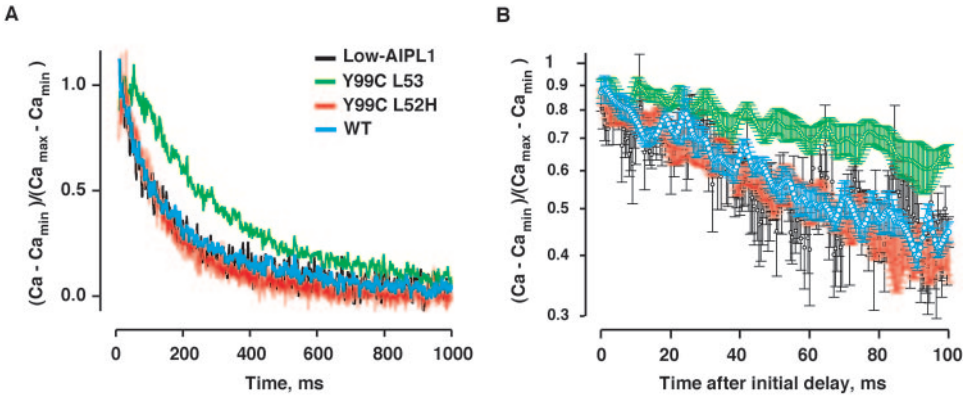

FIGURE 8. Dynamics of intracellular free Ca^{2+} in single rods of low-AIPL1, Y99C L53, L52H, and WT mice. Intracellular Ca^{2+} was measured with fluo-5F, a Ca^{2+} fluorescent dye. The initial fluorescence excited by laser stimulation of rods filled with fluo-5F probed the intracellular concentration of free Ca^{2+} in darkness. The laser stimulation used for excitation of fluo-5F closed all the cGMP-gated channels and sent the rod into saturation. After a slight delay, fluorescence declined, reflecting the light-induced fall in Ca^{2+}. (**A**) Delay in the light-induced decline of Ca^{2+} in Y99C L53 rods. The fluorescence was calibrated and converted to Ca^{2+} concentration for individual rods. For the purposes of this analysis, minimal Ca^{2+} concentration was taken at 1500 ms. A 4-ms offset was removed from the records which were low pass filtered with an eight-pole Bessel at the time of acquisition. Records were digitally filtered at 116 Hz, normalized and then averaged. The average value for the delay determined in individual rods of a given type is listed in Table 3. (**B**) Slower rate of intracellular Ca^{2+} decline in L53 rods. Normalized traces for individual rods were shifted along the abscissa to align the moment when $(Ca^{2+} - Ca^{2+}_{min})/(Ca^{2+}_{max} - Ca^{2+}_{min})$ declined to 0.9. Traces for rods of a given type (low-AIPL1, $n = 12$; Y99C L53, $n = 10$; Y99C L52H, $n = 10$; WT, $n = 21$) were then averaged and plotted on a logarithmic ordinate. Error bars, SEM.

totransduction efficiency is in good agreement with 20% to 50% of the transducins becoming entangled with an RGS9 instead of binding PDE. The situation would occur less than 14% of the time in normal rods but would occur just as often in normal cones, where the ratio of RGS9 to PDE approaches 1.[45] Indeed, no improvement in the efficiency of rod phototransduction was apparent in mice lacking RGS9,[29] but sensitivity of the mid-wavelength–sensitive cone pathway increased approximately twofold.[47]

Finally, the reduced rising phase of the photoresponse was unlikely to have been caused by an effect of high Ca^{2+} or cGMP in darkness, because the initial segment of the photoresponse was normal in Y99C rods. The most probable explanation is that fewer transducins were activated or that a greater fraction of transducins failed to activate PDE.

Slower Response Recovery in Low-AIPL1 Rods

Basal PDE activity plays a key role in setting the time course of photoresponse recovery.[48] Because basal PDE activity stems from the spontaneous activity of PDE molecules,[49] it should be ≥3.4- to 5-fold lower in low-AIPL1 rods. However, in modeling the single-photon response, decreased basal PDE activity alone did not account for the full slowing of response recovery in low-AIPL1 rods (Fig. 9 and Appendix). Also, the large τ_c for low-AIPL1 rods (Fig. 1C) reflected a slower shutoff of either rhodopsin or transducin.[25,26] Photoresponse recovery slows with a reduction in rhodopsin kinase expression[29] and speeds up after knockout of recoverin,[50] which mediates Ca^{2+}-dependent inhibition of rhodopsin shutoff. Before significant degeneration, rhodopsin kinase and recoverin levels are normal in AIPL1 knockout[7] and low-AIPL1 retinas[6] (e.g., Fig. 5B). Intracellular localization of rhodopsin kinase is also normal in low-AIPL1 rods. τ_c was unaffected in Y99C rods, and so differences in dark-adapted Ca^{2+} levels did not greatly affect recoverin-mediated inhibition of rhodopsin shutoff. The slow τ_c in low-AIPL1 rods was not caused by their failure to reach the normal light-induced Ca^{2+} minimum, because the deviation in Ca^{2+} occurred many seconds after flash, long after our measure-

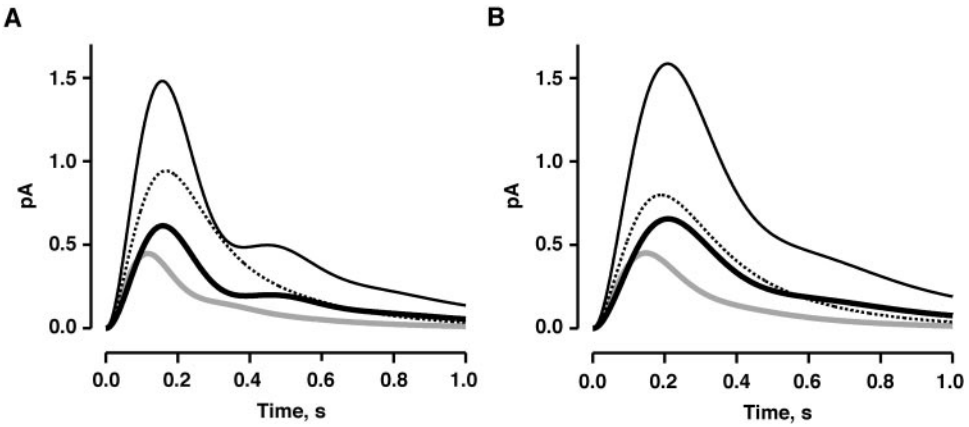

FIGURE 9. Simulated single-photon responses of low-AIPL1 (*thick* and *thin continuous black lines*), Y99C L52H (*dashed lines*) and WT (*gray lines*) rods. Rhodopsin's activity declined exponentially after a 100-ms delay, with a time constant of 270 ms, except for low-AIPL1 rods, where the time constant was set to 430 ms. PDE decay was several times faster. Reversal of the time constants for rhodopsin and PDE shutoffs gave similar results. A 150-ms time constant was used for $Na^+/K^+,Ca^{2+}$ exchange. The R_{max} was 15 pA for WT rods and 18.75 pA for mutant rods. Ca^{2+} in darkness was set to 270 nM in mutant rods and 210 nM in WT rods. In the light, it was set to 78 nM in low-AIPL1, to 39 nM in Y99C, and to 36 nM in WT rods. Although a range of 46 to 70 nM was found for the $K_{m,Ca}$ of the guanylate cyclase activity for low-AIPL1 and WT retinas at 0.9 mM free Mg^{2+} (Fig. 7 and Ref. 14), a value of 200 nM was used, on the grounds that free Mg^{2+} in rods may have been higher under our recording conditions.[37,38] The value was increased twofold to 400 nM, for Y99C L52H rods. A Hill coefficient of 3.7[39] was used for the Ca^{2+} dependence of guanylate cyclase activity in (**A**). Because a Hill coefficient as high as 3.7 has never been observed in biochemical assays, simulations with a Hill coefficient of 2 for WT and low-AIPL1, and a Hill coefficient of 1 for Y99C are shown in (**B**). The lower Hill coefficients enlarged the responses, and so the rhodopsin activities were adjusted to equate the WT responses in (**A**) and (**B**). The simulated responses overestimated the amplitude of the low-AIPL1 rod response and lacked the reduction in the slope of the rising phase (*thin black lines*). Closer matches to the experimental observations were obtained after decreasing the light-activated cGMP hydrolysis (*thick black lines*).

ments of response saturation time. Thus, rhodopsin shutoff in low-AIPL1 rods did not appear to be sluggish. Evidence is lacking for any interaction between AIPL1 and the α-subunit of transducin or RGS9, but the defective shutoff of activated transducin cannot yet be excluded.

In conclusion, low PDE levels delay the onset and compromise the amplification of phototransduction by impairing transducin-PDE binding. The slow photoresponse recovery and elevated Ca^{2+} level after light exposure are not well explained by a simple reduction in PDE or by higher than normal cGMP and Ca^{2+} in darkness. We suggest that besides PDE, AIPL1 directly or indirectly affected at least one other phototransduction cascade component.

APPENDIX

The Rieke and Baylor model[49] for the phototransduction was applied to gain a better understanding of the effects of changing the Ca^{2+} sensitivity of guanylate cyclase and lowering PDE expression on the single-photon response of mutant rods. The model treats the rod outer segment as a well-stirred volume with negligible dynamic Ca^{2+} feedback on the cGMP-gated channel or on rhodopsin lifetime.

PDE activity changes on exposure to light according to

$$\frac{dP(t)}{dt} = \sigma R(t) - k_{\mathrm{PDE}}[P(t) - \beta_{\mathrm{PDE}}], \qquad (A1)$$

where R is the light-activated rhodopsin activity, σ converts R to PDE activation, P is the total PDE activity, β_{PDE} is the basal PDE activity, and k_{PDE} is the rate with which light-activated PDE activity shuts off. The concentration of cGMP, $G(t)$, changes whenever there is an imbalance between its rate of synthesis, γ, and its rate of hydrolysis,

$$\frac{dG(t)}{dt} = \gamma(t) - P(t)G(t). \qquad (A2)$$

The rate of synthesis of cGMP varies as a Hill function of Ca, the free $[Ca^{2+}]_i$:

$$\gamma = \frac{\gamma_{\max}}{1 + (Ca/K_{GC})^n} \qquad (A3)$$

where K_{GC} is the Ca at which cGMP synthesis is half maximal and n is the Hill coefficient. Ca equilibrates as

$$\frac{dCa(t)}{dt} = qbG^3(t) - \beta Ca(t), \qquad (A4)$$

where q converts membrane current to change in Ca, b (0.551 pA μM^{-3}) converts the cube of the cGMP concentration to membrane current and β is the rate constant for $Na^+/K^+,Ca^{2+}$ exchange.

The model nicely reproduced the increase in the single-photon response amplitude as well as the increase in time to peak of the Y99C L52H rod (Fig. 9, dashed lines). Lowered basal PDE activity by three- to fivefold in low-AIPL1 rods had only a small effect on response duration. Inclusion of the slower low-AIPL1 τ_c gave the full prolongation (Fig. 9, thin black lines). The model did not, however, reproduce the observed amplitude of the low-AIPL1 rod response and the reduction in the slope of the rising phase, unless a decrease in light-activated PDE activity was imposed (Fig. 9, thick black lines).

References

1. Arshavsky VY, Lamb TD, Pugh EN Jr. G proteins and phototransduction. *Annu Rev Physiol*. 2002;64:153–187.
2. Makino CL, Wen XH, Lem J. Piecing together the timetable for visual transduction with transgenic animals. *Curr Opin Neurobiol*. 2003;13:404–412.
3. Sokal I, Alekseev A, Palczewski K. Photoreceptor guanylate cyclase variants: cGMP production under control. *Acta Biochim Pol*. 2003; 50:1075–1095.
4. Duda T, Koch KW. Retinal diseases linked with photoreceptor guanylate cyclase. *Mol Cell Biochem*. 2002;230:129–138.
5. Olshevskaya EV, Ermilov AN, Dizhoor AM. Factors that affect regulation of cGMP synthesis in vertebrate photoreceptors and their genetic link to human retinal degeneration. *Mol Cell Biochem*. 2002;230:139–147.
6. Liu X, Bulgakov OV, Wen XH, et al. AIPL1, the protein that is defective in Leber congenital amaurosis, is essential for the biosynthesis of retinal rod cGMP phosphodiesterase. *Proc Natl Acad Sci USA*. 2004;101:13903–13908.
7. Ramamurthy V, Niemi GA, Reh TA, Hurley JB. Leber congenital amaurosis linked to AIPL1: a mouse model reveals destabilization of cGMP phosphodiesterase. *Proc Natl Acad Sci USA*. 2004;101: 13897–13902.
8. Sohocki MM, Bowne SJ, Sullivan LS, et al. Mutations in a new photoreceptor-pineal gene on 17p cause Leber congenital amaurosis. *Nat Genet*. 2000;24:79–83.
9. Sohocki MM, Perrault I, Leroy BP, et al. Prevalence of AIPL1 mutations in inherited retinal degenerative disease. *Mol Genet Metab*. 2000;70:142–150.
10. Payne AM, Downes SM, Bessant DA, et al. A mutation in guanylate cyclase activator 1A (GUCA1A) in an autosomal dominant cone dystrophy pedigree mapping to a new locus on chromosome 6p21.1. *Hum Mol Genet*. 1998;7:273–277.
11. Dizhoor AM, Boikov SG, Olshevskaya EV. Constitutive activation of photoreceptor guanylate cyclase by Y99C mutant of GCAP-1: possible role in causing human autosomal dominant cone degeneration. *J Biol Chem*. 1998;273:17311–17314.
12. Sokal I, Li N, Surgucheva I, et al. GCAP1 (Y99C) mutant is constitutively active in autosomal dominant cone dystrophy. *Mol Cell*. 1998;2:129–133.
13. Wilkie SE, Newbold RJ, Deery E, et al. Functional characterization of missense mutations at codon 838 in retinal guanylate cyclase correlates with disease severity in patients with autosomal dominant cone-rod dystrophy. *Hum Mol Genet*. 2000;9:3065–3073.
14. Olshevskaya EV, Calvert PD, Woodruff ML, et al. The Y99C mutation in guanylyl cyclase-activating protein 1 increases intracellular Ca^{2+} and causes photoreceptor degeneration in transgenic mice. *J Neurosci*. 2004;24:6078–6085.
15. Dizhoor AM, Ray S, Kumar S, et al. Recoverin: a calcium sensitive activator of retinal rod guanylate cyclase. *Science*. 1991;251:915–918.
16. Koch KW, Stryer L. Highly cooperative feedback control of retinal rod guanylate cyclase by calcium ions. *Nature*. 1988;334:64–66.
17. Hurley JB, Dizhoor AM. Heterologous expression and assays for photoreceptor guanylyl cyclases and guanylyl cyclase activating proteins. *Methods Enzymol*. 2000;315:708–717.
18. Wang Z, Wen XH, Ablonczy Z, et al. Enhanced shutoff of phototransduction in transgenic mice expressing palmitoylation-deficient rhodopsin. *J Biol Chem*. 2005;280:24293–24300.
19. Adams RA, Liu X, Williams DS, Newton AC. Differential spatial and temporal phosphorylation of the visual receptor, rhodopsin, at two primary phosphorylation sites in mice exposed to light. *Biochem J*. 2003;374:537–543.
20. Calvert PD, Govardovskii VI, Krasnoperova N, et al. Membrane protein diffusion sets the speed of rod phototransduction. *Nature*. 2001;411:90–94.
21. Bligh EG, Dyer WJ. A rapid method of total lipid extraction and purification. *Can J Biochem Physiol*. 1959;37:911–917.
22. Morrison WR, Smith LM. Preparation of fatty acid methyl esters and dimethylacetals from lipids with boron fluoride–methanol. *J Lipid Res*. 1964;5:600–608.

23. Anderson RE, Maude MB, Acland G, Aguirre GD. Plasma lipid changes in PRCD-affected and normal miniature poodles given oral supplements of linseed oil. Indications for the involvement of n-3 fatty acids in inherited retinal degenerations. *Exp Eye Res*. 1994; 58:129–137.
24. Martin RE, Rodriguez de Turco EB, Bazan NG. Developmental maturation of hepatic n-3 polyunsaturated fatty acid metabolism: supply of docosahexaenoic acid to retina and brain. *J Nutr Biochem*. 1994;5:151–160.
25. Pepperberg DR, Cornwall MC, Kahlert M, et al. Light-dependent delay in the falling phase of the retinal rod photoresponse. *Vis Neurosci*. 1992;8:9–18.
26. Nikonov S, Engheta N, Pugh EN Jr. Kinetics of recovery of the dark-adapted salamander rod photoresponse. *J Gen Physiol*. 1998; 111:7–37.
27. Pugh EN Jr, Lamb TD. Amplification and kinetics of the activation steps in phototransduction. *Biochim Biophys Acta*. 1993;1141: 111–149.
28. Lamb TD. Stochastic simulation of activation in the G-protein cascade of phototransduction. *Biophys J*. 1994;67:1439–1454.
29. Chen CK, Burns ME, He W, et al. Slowed recovery of rod photoresponse in mice lacking the GTPase accelerating protein RGS9–1. *Nature*. 2000;403:557–560.
30. Liang Y, Fotiadis D, Maeda T, et al. Rhodopsin signaling and organization in heterozygote rhodopsin knockout mice. *J Biol Chem*. 2004;279:48189–48196.
31. Cagianut B, Sandri G, Zilla P, Theiler K. Studies on hereditary retinal degeneration: the rd gene in the mouse. *Graefes Arch Clin Exp Ophthalmol*. 1985;223:16–22.
32. Mendez A, Burns ME, Sokal I, et al. Role of guanylate cyclase-activating proteins (GCAPs) in setting the flash sensitivity of rod photoreceptors. *Proc Natl Acad Sci USA*. 2001;98:9948–9953.
33. Howes KA, Pennesi ME, Sokal I, et al. GCAP1 rescues rod photoreceptor response in GCAP1/GCAP2 knockout mice. *EMBO J*. 2002;21:1545–1554.
34. Raport CJ, Lem J, Makino C, et al. Downregulation of cGMP phosphodiesterase induced by expression of GTPase-deficient cone transducin in mouse rod photoreceptors. *Invest Ophthalmol Vis Sci*. 1994;35:2932–2947.
35. Lyubarsky A, Nikonov S, Pugh EN Jr. The kinetics of inactivation of the rod phototransduction cascade with constant Ca^{2+}_i. *J Gen Physiol*. 1996;107:19–34.
36. Hetling JR, Pepperberg DR. Sensitivity and kinetics of mouse rod flash responses determined in vivo from paired-flash electroretinograms. *J Physiol*. 1999;516:593–609.
37. Chen C, Nakatani K, Koutalos Y. Free magnesium concentration in salamander photoreceptor outer segments. *J Physiol*. 2003;553: 125–135.
38. Peshenko IV, Dizhoor AM. Guanylyl cyclase-activating proteins (GCAPs) are Ca^{2+}/Mg^{2+} sensors: implications for photoreceptor guanylyl cyclase (RetGC) regulation in mammalian photoreceptors. *J Biol Chem*. 2004;279:16903–16906.
39. Burns ME, Mendez A, Chen J, Baylor DA. Dynamics of cyclic GMP synthesis in retinal rods. *Neuron*. 2002;36:81–91.
40. Capovilla M, Cervetto L, Torre V. Antagonism between steady light and phosphodiesterase inhibitors on the kinetics of rod photoresponses. *Proc Natl Acad Sci USA*. 1982;79:6698–6702.
41. Sandberg MA, Pawlyk BS, Crane WG, Schmidt SY, Berson EL. Effects of IBMX on the ERG of the isolated perfused cat eye. *Vision Res*. 1987;27:1421–1430.
42. Ramamurthy V, Roberts M, van den Akker F, et al. AIPL1, a protein implicated in Leber's congenital amaurosis, interacts with and aids in processing of farnesylated proteins. *Proc Natl Acad Sci USA*. 2003;100:12630–12635.
43. He W, Cowan CW, Wensel TG. RGS9, a GTPase accelerator for phototransduction. *Neuron*. 1998;20:95–102.
44. Hu G, Wensel TG. R9AP, a membrane anchor for the photoreceptor GTPase accelerating protein, RGS9–1. *Proc Natl Acad Sci USA*. 2002;99:9755–9760.
45. Zhang X, Wensel TG, Kraft TW. GTPase regulators and photoresponses in cones of the eastern chipmunk. *J Neurosci*. 2003;23: 1287–1297.
46. Skiba NP, Hopp JA, Arshavsky VY. The effector enzyme regulates the duration of G protein signaling in vertebrate photoreceptors by increasing the affinity between transducin and RGS protein. *J Biol Chem*. 2000;275:32716–32720.
47. Lyubarsky AL, Chen CK, Naarendorp F, et al. RGS9–1 is required for normal inactivation of mouse cone phototransduction. *Mol Vis*. 2001;7:71–78.
48. Nikonov S, Lamb TD, Pugh EN Jr. The role of steady phosphodiesterase activity in the kinetics and sensitivity of the light-adapted salamander rod photoresponse. *J Gen Physiol*. 2000; 116:795–824.
49. Rieke F, Baylor DA. Origin of reproducibility in the responses of retinal rods to single photons. *Biophys J*. 1998;75:1836–1857.
50. Makino CL, Dodd RL, Chen J, et al. Recoverin regulates light-dependent phosphodiesterase activity in retinal rods. *J Gen Physiol*. 2004;123:729–741.